# On the plasmon-assisted detection of a 1585 $cm^{-1}$ mode in the 532 nm Raman spectra of crystalline α-$Fe_2O_3$/polycrystalline NiO core/shell nanofibers

Saveria Santangelo,[1,*,#] Muhammad Hamid Raza,[2,#] Nicola Pinna[2], and Salvatore Patanè[3]

[1] Dipartimento di Ingegneria Civile, dell'Energia, dell'Ambiente e dei Materiali (DICEAM), Università "Mediterranea", Loc. Feo di Vito, 89122 Reggio Calabria, Italy

[2] Institut für Chemie and IRIS Adlershof, Humboldt-Universität zu Berlin, Brook-Taylor Str. 2, 12489 Berlin, Germany

[3] Dipartimento di Scienze Matematiche e Informatiche, Scienze Fisiche e Scienze della Terra (MIFT), Università di Messina, Viale Stagno d'Alcontres 31, 98166 Messina, Italy

**Abstract.** Crystalline hematite/polycrystalline nickel oxide (α-$Fe_2O_3$/NiO) core/shell nanofibers are prepared by electrospinning and calcination, followed by a varying number (100–1150) of atomic layer deposition cycles of NiO. The deposition of the conformal NiO layer leads to the passivation of the surface states and the appearance of a photoluminescence band in the micro-Raman spectra excited by 532 nm laser. As a continuous NiO layer is formed, a peak, possibly arising from a two-magnon mode, appears at 1585 $cm^{-1}$. The detection of the peak, which is not observed in the spectra excited by a 633 nm laser, is assisted by the surface plasmon at around 510 nm introduced by the polycrystalline NiO layer, due to the electron doping induced by coordination-defects at its edge-rich surface.

Thanks to its low cost, great stability, biocompatibility, ecofriendliness and appealing physicochemical properties, hematite (α-$Fe_2O_3$) is extensively used in a myriad of very different applications, ranging from energy conversion and storage to air purification.[1–4] Its narrow band gap (2.0–2.2 eV), suitable for efficient absorption of visible light, makes of nanostructured α-$Fe_2O_3$ the most popular photoanode material to catalyze the oxygen evolution reaction in photoelectrochemical (PEC) water splitting.[1,2] Hematite has also interesting magnetic properties.[5] In the latest years, high aspect-ratio nanohematites, such as nanofibers, nanorods and nanotubes, have been focus of extensive studies in view of applications exploiting these properties.[6–10]

Recently, Lebrun et al.[11] have demonstrated the long-distance propagation of spin currents through a hematite single crystal by using the spin Hall effect for spin injection. Conversely, exciting magnons with an optical probe is a challenging task. Mikhaylovskiy et al.[12] have observed terahertz emission by spin resonances induced in α-$Fe_2O_3$ by the ultrafast modulation of the super-exchange interaction via laser pulses. Rodriguez et al.[13] have successfully excited spin waves in hematite nanoparticles by using continuous optical radiation, as proved by the appearance of a two-magnon (2M) mode at ~1584 $cm^{-1}$ in the tip- and surface-enhanced Raman (TERS and SERS) spectra. The magnon excitation is due to the phonon-mediated coupling of the spins with the strongly localized electromagnetic field near the metallic nanostructure, while the plasmonic enhancement allows for the band detection.[13]

Nickel oxide (NiO), a wide band gap (3.6−4.4 eV) *p*-type semiconductor, is a low-cost, non-toxic material attracting increasing attention in antimicrobial[14] and gas-sensing applications.[15,16] It is also used to improve the PEC performance of hematite: it has been reported that the α-$Fe_2O_3$/NiO *n*/*p*-heterojunction allows for a more effective separation of the photogenerated electron-hole pairs and a reduction of their recombination rate.[17–19] Recently, Lin et al.[20] have shown that, in a two-dimensional amorphous nickel oxide (2D *a*-NiO) layer, the surface plasmon resonance (SPR) introduced at around 530 nm by the the amorphization and 2D effect-induced electron doping makes the resulting material able to boost the photocatalytic activity for solar $H_2$ evolution through the SPR-mediated charge releasing.

This work deals with α-$Fe_2O_3$/NiO core/shell nanofibers (CSNFs) and reports on the detection of a mode at 1585 $cm^{-1}$ in their Raman spectra excited by 532 nm optical radiation thanks to the plasmonic enhancement by the polycrystalline NiO shell.

* **Corresponding author**
E-mail address: saveria.santangelo@unirc.it (Prof. Saveria Santangelo)
**# Author Contributions**
S.S. and M.H.R. contributed equally to this work.

The $\alpha$-$Fe_2O_3$ core was prepared by electrospinning (ES) followed by calcination, as illustrated in detail in a previous work (Fig. S1a).[3] The thin (1.3–28 nm) NiO shell was obtained via atomic layer deposition (ALD), the technique of choice to develop highly conform and uniform coatings.[21]

Briefly, a homogenous suspension of $\alpha$-$Fe_2O_3$ NFs in ethanol was drop-casted on an Al-foil and dried at room temperature (RT). ALD was carried out in a commercial ALD reactor by Arradiance as reported elsewhere.[10] Nickelocene acted as a metal precursor; ozone was used as an oxygen source (Fig. S1b). The ALD was carried out at 200 °C, whereas the time for precursor's pulses and exposures time was adjusted as 1.5 s/40 s and 0.2 s/30 s for nickelocene and ozone, respectively. The thickness of the NiO-shell layer was controlled by varying the number of ALD cycles (100–1150). The comprehensive of the NiO ALD procedure is described in our previous reports.[15,16]

The CSNFs were coded as $HN_N$, with $N$ standing for the number of ALD cycles. After ALD, they were wiped off from the Al-foil and analyzed. High-resolution transmission electron microscopy (HRTEM), high-angle annular dark-field scanning transmission electron microscopy (HAADF-STEM) and energy dispersive X-ray analysis (EDX) elemental mappings were carried out via an FEI Talos F200S scanning/transmission electron microscope (S/TEM), operated at 200 kV. Raman scattering measurements were performed, at RT, by a confocal microscope (NTEGRA - Spectra SPM from NT-MDT) coupled to 532 or 633 nm lasers. The scattered light from the sample was collected by means of a 100X (0.75 NA) Mitutoyo objective and detected by a cooled CCD Camera (ANDOR iDus). The laser power at the sample surface was 60 μW to prevent unintentional annealing of the samples. Diffuse reflectance NIR-VIS-UV spectra were recorded using a PerkinElmer LAMBDA 950 UV/vis spectrophotometer equipped with a 150 mm integrating sphere. Powdered samples were measured by mixing them with a small amount of $BaSO_4$.

Figure S2 shows the texture and morphology of the pristine $\alpha$-$Fe_2O_3$ and NiO-coated NFs as resulting from TEM analysis. As pointed out in previous studies,[3,10] hematite NFs exhibit the coral-like architecture peculiar to the electrospun iron oxide NFs[4] (Fig. S2a). They consist of interconnected rounded and smooth single-crystal (SC) or quasi-single-crystal (QSC) $\alpha$-$Fe_2O_3$ grains[10] about 65 nm in size.[3]

The ALD process does not introduce any architecture changes, but a conformal coating of the grains (Fig. S2b–g). For $N < 100$, only small NiO particles are present; with increasing $N$, they grow and coalesce giving rise to a conformal ($N \geq 300$) and continuous ($N \geq 500$) shell layer, until filling of the voids between the grains ($N \geq 650$). The shell thickness, as estimated from the HAADF-STEM images of the CSNFs, increases from 1.3 to 28.5 nm with $N$ varying from 100 to 1150 (not shown here). The thin NiO shell layer is polycrystalline in nature and has rock-salt (cubic) structure as confirmed by XRD (Fig. S4b) and SAED patterns (not shown here,[15,16]); its surface is very rich in edges, which implies a large amount of under-coordinated Ni atoms ($Ni^0$-like defects).[20,22]

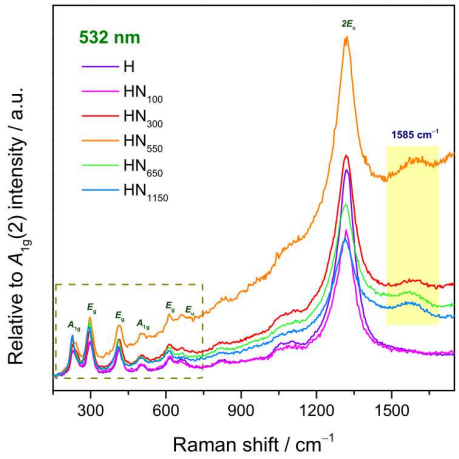


**Fig. 1.** Micro-Raman spectra for 532 nm laser light excitation. The spectra are normalized to the amplitude of the $A_{1g}(2)$ peak at ~500 $cm^{-1}$ that is insensitive to the nanoparticle and/or crystallite size. The Raman-allowed modes of the $\alpha$-$Fe_2O_3$ core are marked by a dashed rectangle; the two-magnon peak is yellow-highlighted.

**Figure 1** shows the micro-Raman spectra of the NFs. No obvious peak ascribable to polycrystalline NiO is detected,[23,24] regardless of the thickness of the shell layer most probably due to the small scattering volume. Below 750 $cm^{-1}$ the peaks originating from the Raman-allowed phonon modes of the $\alpha$-$Fe_2O_3$ core are detected together with the $E_u$ peak (at ~660 $cm^{-1}$), activated by disorder (defects, heteroatoms, grain size) in the hematite lattice.[3,10,25]

The very strong asymmetrical band assigned to the overtone of the $E_u$ mode (at ~1320 cm$^{-1}$), dominates the higher frequency region.[26,27] For $N \geq 300$, the peaks are superimposed to a photoluminescence (PL) background as the continuous conformal NiO shell formed behaves as a passivation layer and (with no need of annealing) promotes the partial suppression of the surface trap states in hematite with strain release and appearance of a band at ~2 eV (Fig. S5), in line with literature reports[28–32] and results of a previous study.[10]

The formation of a continuous conformal NiO shell is further accompanied by the appearance of an additional contribution (yellow-highlighted in Fig. 1) on the tail of the $2E_u$ mode, between 1480–1690 cm$^{-1}$. The peak is generally not observed in hematite[3,27] and hematite-based composites.[10] It cannot be ascribed to the NiO 2M mode, which, at RT, is detected at ~1460 and 1500 cm$^{-1}$ in very large-sized crystals and NiO SC, respectively.[23] A peak located at the same frequency was detected by Rodriguez et al.[13] in the SERS and TERS spectra of hematite nanoparticles by exploiting the enhancement by the plasmonic metal and it was ascribed to a 2M excitation in the hematite lattice.[13,26] Hence, in the following, the peak at 1585 cm$^{-1}$ will be referred as the 2M peak, although, in principle, it cannot be excluded that it has a different origin (e.g. interface mixed mode due to strain coupling between the NiO and the $\alpha$-$Fe_2O_3$ core on the very interface).

Recently, Lin et al.[20] have reported on a SPR at around 530 nm in a 2D *a*-NiO layer. They have proposed that the introduction of the SPR is due to the increased electron doping resulting from the amorphization and 2D effect-induced under-coordinated Ni atoms. Amorphization-induced increased light absorption in the visible region (360–500 nm) has been reported also by Sun et al.[33] for an ultrathin *a*-NiO layer.

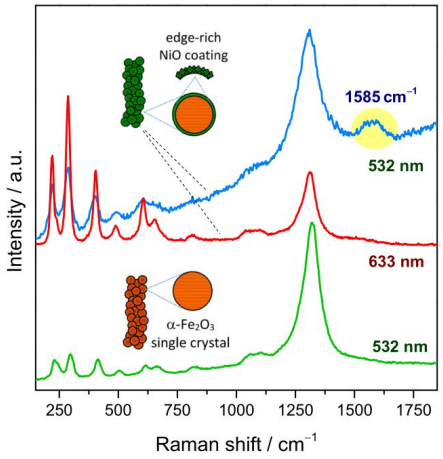


**Fig. 2.** Micro-Raman spectra of sample $HN_{550}$ for 532 nm and 633 nm excitation. The 532 nm spectrum of bare $\alpha$-$Fe_2O_3$ NFs is reported for comparison.

These results suggest that, in the present case, the 2D conformal NiO shell might behave as a plasmonic layer allowing for the detection of the 2M-peak since electron doping induced by coordination-defects at its edge-rich surface, besides compensating the intrinsic hole doping completely, may produce a large amount of free electrons.[20] In order to test these hypotheses, first, the investigated CSNFs were annealed at 200 and 300°C for 24 h in air trying to oxidize the Ni-defects. The annealing at the lower temperature only partly oxidizes the Ni-defects, which results in weaker intensity of the peak at 1585 cm$^{-1}$ (Fig. S6); conversely, after the annealing at the higher temperature, the Ni-defect oxidation is complete and the peak is no longer visible (Fig. S6). The same occurs if the scattering is measured after 5 min local exposure to laser light with 0.6 mW power at the sample surface (Fig. S6). Raman scattering is then excited by a different wavelength (**Fig. 2**). As shown in the case of sample $HN_{550}$, no peak at 1585 cm$^{-1}$ is detected for 633 nm excitation, like in bare $\alpha$-$Fe_2O_3$ NFs, supporting the possibility of a plasmonic assistance by the NiO shell for the 2M-peak detection, in agreement with latest reports on 2D defective and amorphous semiconductor compounds as plasmonic materials with improved performance with respect to conventional noble metals.[34,35]

In order to ascertain the occurrence of a SPR, the NIR-VIS-UV diffuse reflectance spectra are recorded (**Fig. 3**). The results obtained are in full agreement with the results reported in literature for hematite.[36,37] Then, following Li et al.,[38] the light absorption enhancement in the 400–600 nm spectral region from plasmonic 2D conformal NiO shell on the $\alpha$-$Fe_2O_3$ core is evidenced by subtracting the reflectance curve of hematite with those of CSNFs (Fig. S7).

Actually, by fitting the as-obtained curves (inset of Fig. 3), the occurrence of SPR at around 510 nm (and, hence, the SERS effect due to the local electromagnetic field enhancement of the plasmonic NiO shell in Raman spectra) is demonstrated. As expected, with increasing NiO layer thickness, the plasmon moves towards higher wavelength (Fig. S8a); besides, as the NiO layer loses the 2D nature due to the filling of the inter-grain voids, its relative intensity starts decreasing (Fig. S7b). The estimation of the carrier density from the SPR frequency, based on the Drude model,[20] gives a value ($8.6 \cdot 10^{21}$ $cm^{-3}$ for sample $HN_{550}$) fully compatible with those reported in the literature for the above mentioned *a*-NiO layers with plasmonic properties.[20,33]

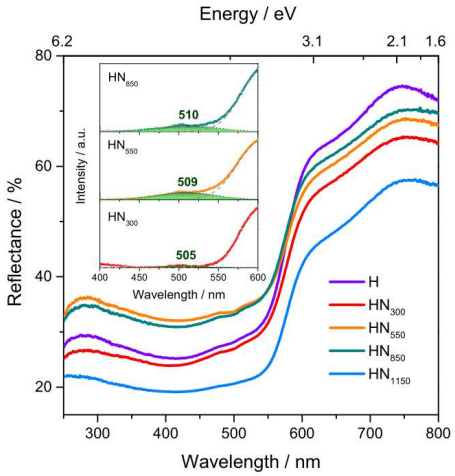


**Fig. 3.** NIR-VIS-UV diffuse reflectance spectra. Inset: light absorption enhancement in the 400–600 nm spectral region from plasmonic 2D conformal NiO shell on the $\alpha$-$Fe_2O_3$ core.

Finally, a further proof that the NiO shell layer is responsible for the 2M mode detection comes from the comparison with $\alpha$-$Fe_2O_3$ CSNFs ALD-coated with a different oxide. Figure S9 shows the Raman spectra of $\alpha$-$Fe_2O_3$ CSNFs coated with NiO and $SiO_2$ layers having comparable thickness. No peak at 1585 $cm^{-1}$ is detected in the spectra of $\alpha$-$Fe_2O_3$/$SiO_2$ CSNFs.[10]

In the present study, we demonstrate that a 2D polycrystalline NiO shell deposited by atomic layer deposition onto electrospun crystalline $\alpha$-$Fe_2O_3$ NFs, because of a defect-induced SPR at ~510 nm, acts as a plasmonic layer allowing for the detection of a two-magnon mode of $\alpha$-$Fe_2O_3$ at 1585 $cm^{-1}$ in the micro-Raman spectra excited at 532 nm.

Since ALD allows for a very fine-tuning of the deposited oxide layers, the reported results pave the way to the controlled synthesis of plasmonic oxide-based nanomaterials, which are gathering attention as a very promising alternative to traditional noble metals. Moreover, they could be of practical interest in the field of solar-driven electrochemical water splitting with the NiO layer acting as a plasmonic material for the light harvesting, while the investigated CSNFs could be engineered for the optical generation and control of spin waves in spintronics.

**Supplementary Material**

Sketch of the experimental procedure for the synthesis of $\alpha$-$Fe_2O_3$/*a*-NiO CSNFs; BF-TEM micrographs and EDX elemental mapping; EDX spectra; XRD patterns; Photoluminescence spectra and *N*-dependence of its relative intensity; Micro-Raman spectra of sample $HN_{300}$ before and after 24h annealing in an oxygen rich atmosphere at 300 °C; NIR-VIS-UV diffuse reflectance spectra and light absorption enhancement from plasmonic 2D conformal NiO shell; Wavelength and relative intensity of the NiO plasmon; Micro-Raman spectra of $\alpha$-$Fe_2O_3$ CSNFs ALD-coated with NiO and $SiO_2$ layers having comparable thickness.

**Acknowledgments**

We thankfully acknowledge C. Erdmann for electron microscopy measurements and A. Ponti for the stimulating discussion on the properties of antiferromagnetic nanomaterials. Y. Wang is thanked for his help in the UV-VIS measurements.

**Availability of data**

The data that support the findings of this study are available from the corresponding author upon reasonable request.

**References**


1 K. Sivula, F. Le Formal, and M. Grätzel, ChemSusChem, **4**, 432 (2011).
2 D. K. Bora, A. Braun, and E. C. Constable, Energy & Environm. Sci. **6**, 407 (2013).
3 M. Fiore, G. Longoni, S. Santangelo, F. Pantò, S. Stelitano, P. Frontera, P. Antonucci, and R. Ruffo, Electrochim. Acta **269**, 367 (2018).
4 J. Balbuena, M. Cruz-Yusta, A. L. Cuevas, F. Martín, A. Pastor, R. Romero, and L. Sánchez, J. Alloys Comp **797**, 166 (2019).
5 A. H. Morrish, *Canted Antiferromagnetism: Hematite* (World Scientific, Singapore, SGP, 1994).
6 Y. Zhu, J. C. Zhang, J. Zhai, and L. Jiang, Thin Solid Films **510**, 271 (2006).
7 Y. Zhao, C. W. Dunnill, Y. Zhu, D. H. Gregory, W. Kockenberger, Y. Li, W. Hu, I. Ahmad, and D. G. McCartney, Chem. Mater. **19**, 916 (2007).
8 C. Eid, D. Luneau, V. Salles, R. Asmar, Y. Monteil, A. Khoury, and A. Brioude, J. Phys. Chem. C **115**, 17643 (2011).
9 C. Han, J. Shi, S. Yang, Y. Wang, K. Xie, X. Song, H. Liu, A. Cai, and S. Yun, Appl. Surf. Sci. **507**, 145179 (2020).
10 A. Ponti, M. H. Raza, F. Pantò, A. M. Ferretti, C. Triolo, S. Patanè, N. Pinna, S. Santangelo, Langmuir, **36**, 1305 (2020).
11 R. Lebrun, A. Ross, S. A. Bender, A. Qaiumzadeh, L. Baldrati, J. Cramer, A. Brataas, R. A. Duine, and M. Kläui, Nature **561**, 222 (2018).
12 R. V. Mikhaylovskiy, E. Hendry, A. Secchi, J. H. Mentink, M. Eckstein, A. Wu, R.V. Pisarev, V.V. Kruglyak, M.I. Katsnelson, Th. Rasing, and A. V. Kimel, Nature Commun. **6**, 1 (2015).
13 R. D. Rodriguez, E. Sheremet, T. Deckert-Gaudig, C. Chaneac, M. Hietschold, V. Deckert, and D. R. Zahn, Nanoscale, **7**, 9545 (2015).
14 G. T. Anand, R. Nithiyavathi, R. Ramesh, S. J. Sundaram, and K. Kaviyarasu, Surf. Interf. **18**, 100460 (2020).
15 M. H. Raza, K. Movlaee, S. G. Leonardi, N. Barsan, G. Neri, and N. Pinna, Adv. Funct. Mater. **30**, 1906874 (2020).
16 M. H. Raza, N. Kaur, E. Comini, and N. Pinna, ACS Appl. Mater. Interf. **12**, 4594 (2020).
17 J. Li, F. Meng, S. Suri, W. Ding, F. Huang, and N. Wu, Chem. Commun. **48**, 8213 (2012).
18 L. Li, H. Dai, D. Luo, S. Wang, and X. Sun, Energy Technol. **4**, 758 (2016).
19 H, Bemana, and S. Rashid-Nadimi, Surf. Interf. **14**, 184 (2019).
20 Z. Lin, C. Du, B. Yan, C. Wang, and G. Yang, Nature Commun. **9**, 1 (2018).
21 N. Pinna, and M. Knez Eds. *Atomic layer deposition of nanostructured materials*. (John Wiley & Sons, Weinheim, 2012), Vol. 1.
22 A. Anspoks, and A. Kuzmin, J. non-cryst. Sol. **357**, 2604 (2011).
23 N. Mironova-Ulmane, A. Kuzmin, I. Steins, J. Grabis, I. Sildos, and M. Pärs, J. Phys.: Conf. Series, **93**, 012039 (2007).
24 C. Mrabet, M. B. Amor, A. Boukhachem, M. Amlouk, and T. Manoubi, Ceramics Int. **42**, 5963 (2016).
25 I. V. Chernyshova, M. F. Hochella Jr, and A. S. Madden, Phys. Chem. Chem. Phys. **9**, 1736 (2007).
26 M. J. Massey, U. Baier, R. Merlin, and W. H. Weber, Phys. Rev. B **41**, 7822 (1990).
27 C. P. Marshall, W. J. Dufresne, and C. J. Rufledt, J. Raman Spectrosc. **51**, 1522 (2020).
28 T. Hisatomi, F. Le Formal, M. Cornuz, J. Brillet, N. Tétreault, K. Sivula, and M. Grätzel, Energy Environm. Sci. **4**, 2512 (2011).
29 R. Liu, Z. Zheng, J. Spurgeon, and X. Yang, Energy Environm. Sci. **7**, 2504 (2014).
30 L. Steier, I. Herraiz-Cardona, S. Gimenez, F. Fabregat-Santiago, J. Bisquert, S. D. Tilley, and M. Grätzel, Adv. Funct. Mater. **24**, 7681 (2014).
31 M. G. Ahmed, I. E. Kretschmer, T. A. Kandiel, A. Y. Ahmed, F. A. Rashwan, and D. W. Bahnemann, ACS Appl. Mater. Interf. **7**, 24053 (2015).
32 M. Forster, R. J. Potter, Y. Yang, Y. Li, and A. J. Cowan, ChemPhotoChem, **2**, 183 (2018).
33 S. Sun, G. Shen, Z. Chen, L. Pan, X. Zhang, and J. J. Zou, Appl. Catal. B **285**, 119798 (2020).
34 W. Liu, Q. Xu, W. Cui, C. Zhu, and Y. Qi, Angew. Int. Ed. Chem. **56**, 1600 (2017).
35 W. Liu, and Q. Xu, Chemistry–A Eur. J. **24**, 13693 (2018).
36 B. Ahmmad, K. Leonard, M. S. Islam, J. Kurawaki, M. Muruganandham, T. Ohkubo, and Y. Kuroda, Adv. Powder Technol. **24**, 160 (2013).
37 N. M. A. Rashid, C. Haw, W. Chiu, N. H. Khanis, A. Rohaizad, P. Khiew, and S. A. Rahman, CrystEngComm, **18**, 4720 (2016).
38 J. Li, S. K. Cushing, D. Chu, P. Zheng, J. Bright, C. Castle, A. Manivannan, and N. Wu, J. Mater. Res. ***31***, 1608 (2016).

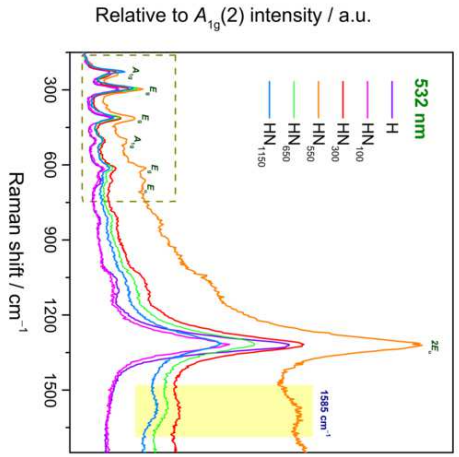

PLEASE CITE THIS ARTICLE AS DOI: 10.1063/5.0050873

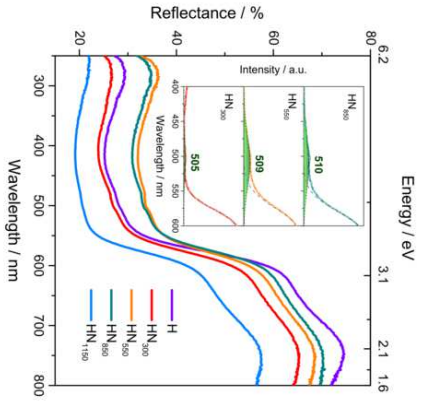

AIP Publishing

Applied Physics Letters ACCEPTED MANUSCRIPT



PLEASE CITE THIS ARTICLE AS DOI: 10.1063/5.0050873